STRUCTURAL ANALYSIS OF A REGENERATIVE FLOW TURBINE FOR LOW-TEMPERATURE ORGANIC RANKINE CYCLE SYSTEMS

Luca Cioccolanti[1,*], Edoardo Mancini[2], Ramin Moradi[1], Emanuele Farotti[3], Marco Sasso[3]

[1] Università eCampus, Centro di Ricerca per l'Energia, l'Ambiente e il Territorio, Novedrate (CO), Italy

[2] Università degli Studi dell'Aquila, Dipartimento di Ingegneria industriale e dell'informazione e di economia, L'Aquila, Italy

[3] Università Politecnica delle Marche, Dipartimento di Ingegneria Industriale e Scienze Matematiche, Ancona, Italy

*Corresponding Author: luca.cioccolanti@uniecampus.it

ABSTRACT

A Regenerative flow turbine (RFT) is an innovative turbomachine based on the momentum exchange between the impeller and the flow resulting in a helical trajectory in the peripheral direction and generating a pulse pressure variation inside the flow. In general, an RFT shows low isentropic efficiencies compared to other kinds of expanders, but the potential low manufacturing cost makes it an alternative expander for low-temperature Organic Rankine Cycle (ORC) applications.
In a previous study carried out by some of the authors, the performances of an RFT for low-grade waste heat recovery (WHR) applications in a non-regenerative ORC system have been preliminarily assessed. In this work, a structural analysis of the same RFT geometry has been performed in ANSYS to evaluate the mechanical stress before its potential manufacturing. More precisely, two different low-cost materials have been investigated namely aluminum and polyphenylene sulfide (PPS), and the most critical parts of the expander identified considering the nominal operating conditions of the ORC system.
The analysis has shown that the maximum tensile strength is reached during the thermal transient phase and it is about 127.4 MPa and 50.8 MPa for aluminum and PPS respectively. Under thermal steady-state conditions, instead, the maximum stress lowers to 42 MPa for aluminum and 40 MPa for PPS. Hence, together with the evaluation of the mechanical stress of the expander in low-temperature applications, the analysis has provided useful insights into the expected power output and the potential dilation of the material, which may result in the critical operation of the impeller.

1 INTRODUCTION

Despite many measures that have been implemented by the industrial sector in the last decades for higher efficiencies of energy systems, a significant potential for reducing CO_2 emissions from the recovery of the huge amount of waste heat from existing industrial facilities has remained intact. According to (Johnson *et al.*, 2008), 20-50 percent of industrial energy consumption is wasted, and 18-30 percent of this waste heat can be further utilized. In general, WHR systems can exploit low-to-medium-grade thermal energy instead of fossil fuels to produce electricity thus reducing fossil fuel consumptions and the related carbon emissions.
Among the different WHR technologies, ORC systems are particularly interesting for their reliability, flexibility, safety, and applicability for low-temperature power generation (Mahmoudi *et al.*, 2018). While at medium (50-300 kW) and large scales (>300 kW) ORCs are a mature and reliable technology, further efforts are still needed to make these systems competitive also at the micro (<10 kW) to small (10-50 kW) scales.
In micro and small-scale ORC systems, the expansion machine represents the key component as far as the performance, reliability, and capital cost are concerned. So far, most of the expanders used in micro-

to-small-scale ORCs are volumetric expanders that were formerly compressors in air conditioning and refrigeration applications and then converted to be used as expanders. Among them, scroll expanders are considered a good choice for ORC systems in the power range of 1-10 kW according to (Dumont *et al.*, 2018). However, scroll expanders are affected by a reduction of their performances at low pressure ratios and mass flow rates. Therefore, the literature review on small-scale ORC systems has revealed the need for reliable and low-cost expanders for WHR applications able to operate also at low flow rates.

In an RFT, part of the flow follows a circular path through the channels, and the remaining part enters the impeller pockets and returns to the channels several times resulting in a helical trajectory of the flow in the peripheral direction creating a pulsive pressure distribution inside the flow. For a given rotational speed, the number of completed swirls of the flow is lower at low flow rates and consequently, the obtained pressure ratio is lower. On the contrary, the isentropic efficiency is higher at a low flow rate. Furthermore, RFTs also inherit some characteristics of positive displacement machines such as reducing pressure ratio by increasing the shaft speed, or their ability to handle two-phase flows making them suitable to operate with few degrees of superheating in micro-scale ORC systems. In addition, RFTs exhibit high-temperature capability, noiseless operation, high reliability, and low manufacturing costs compared with other turbomachines at the same working conditions. Nevertheless, low efficiencies, typically ranging between 35% and 50% (Quail *et al.*, 2010), have restricted the large adoption of RF turbo-machines so far. For these reasons, some authors of the present paper investigated the potential of RFTs to be used in ORC systems for low-grade WHR (Moradi *et al.*, 2020). The authors found that despite such a machine has lower peak isentropic efficiency compared to the scroll expanders, its isentropic efficiency is less sensitive to the pressure ratio thus making it suitable for WHR applications characterized by high fluctuations of the heat source.

As previously mentioned, another advantage of RFTs is their potential low manufacturing cost. Therefore, structural analysis has been performed in ANSYS Mechanical (2021) in this study based on the results of previous computational fluid-dynamic (CFD) studies to properly evaluate the mechanical stress and provide insights into the material selection for its manufacturing.

Hence, the paper is structured as follows: after the introduction, Section 2 described the turbine under investigation together with the methods used. In Section 3 the main results of the analysis are reported while Section 4 concludes.

2 MODELS AND METHODS

2.1 The geometry and the CFD model of the RFT

The geometry of the RFT under investigation is the same as the one considered in a previous study (Moradi *et al.*, 2020) by some of the authors. The main parts of the RFT modeled in this work include the impeller, the casing, the stripper, and the inlet and outlet ports. The impeller consists of a disk having blades on both sides to better balance the axial forces while the casing covers the impeller on both sides thus creating the channels from the inlet to the outlet. The stripper separates the inlet from the outlet of the machine on each side to reduce the leakage flow between them, while a small gap separates the impeller blades from the stripper body to avoid any scraping.

Since a symmetry plane crosses the middle of the impeller, only the halved geometry of the RFT is considered for the CFD simulations in ANSYS® Fluent that is shown in Figure 1.

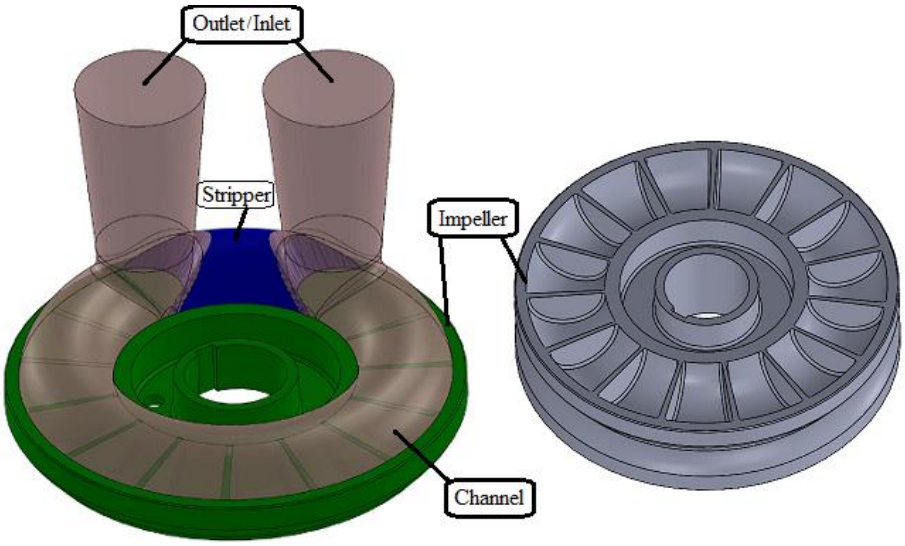

Figure 1: The 3D geometry of the turbine (left) and the impeller (right).

R245fa was considered as the working fluid using the Peng-Robinson real gas model for the density calculations. The considered turbulence model was the Reynolds Stress baseline model (BSL) using the k-ω SST (Shear-Stress Transport) as the initial solution. The pressure-velocity coupling was solved using the PISO scheme, and PRESTO! was chosen for the pressure discretization scheme. The rotation of the impeller was considered using a steady-state model, the Moving Reference Frame (MRF), also known as the Frozen Rotor approach. The inlet temperature was set to a range of values typical of ORC units working with R245fa, while the inlet pressure is part of the results for a given mass flow rate and outlet pressure. The maximum admissible mass flow rate was determined from the CFD results of the RFT by controlling the obtained pressure ratio (PR) and considering the maximum suction pressure of 2 MPa, which corresponds to a maximum PR of about 6.5.

Table 1 reports the imposed boundary conditions and the main results of the model considered for the structural analysis. It is worth noticing that higher mass flow rates are not considered since the RFT efficiency drops, which may not be useful in practice while higher inlet temperatures are not considered to limit the study for low-temperature applications. Indeed, the turbine works with higher efficiencies in lower mass flow rates and pressure ratios; for example, it exhibits an isentropic efficiency of about 44% with a pressure ratio of 1.2 as shown in (Moradi *et al.*, 2020), but the most severe condition is here considered for the sake of the structural analysis.

For the working conditions presented in Table 1, the impeller tip speed is about 20 m/s and the turbine performances are calculated using the dimensionless numbers of compressible flow turbines due to the high Mach number of the gas (Ma>0.5) during the expansion and the non-negligible compressibility effects and variations of the gas density in the studied RFT (Moradi *et al.*, 2019). These dimensionless parameters, which are common for compressible flow turbomachines (Dixon and Hall, 2010), are the reduced blade speed or the blade Mach number (*BM*), the reduced mass flow rate or the capacity ($\dot{m}$), and the specific power or the stage loading (ψ) presented in Equations (1-3) respectively.

$$BM = \frac{wD}{C} \tag{1}$$

where w is the impeller frequency (rad/s), C is the speed of sound in R245fa calculated using the temperature and pressure at the turbine suction, and D is the tip diameter of the impeller.

$$\dot{m} = \frac{\dot{M}\sqrt{C_p T_{0,in}}}{D^2 P_{0,in}} \tag{2}$$

where $\dot{m}$ is the reduced mass flow rate, $\dot{M}$ is the mass flow rate, $P_{0,in}$ and $T_{0,in}$ are respectively the stagnation pressure and temperature at the suction.

$$\psi = \frac{\Delta h_0}{U^2} \tag{3}$$

where U is the impeller velocity. Therefore, the stage loading indicates the amount of the specific work produced in each stage of the turbine for a given impeller speed. The higher the stage loading the higher the work density for the given shaft speed. For more details about the geometrical parameters, the mesh, and the CFD model and its main results, interested readers are invited to see (Moradi et al., 2020).

Table 1: The imposed boundary conditions and the obtained results of the CFD model

Boundary conditions					**Results**				
$\dot{M}$ [kg/s]	T_{in} [K]	P_{out} [MPa]	n [rpm]	P_{in} [MPa]	$\dot{W}_{th}$[kW]	$\eta_{is,tts}$ [%]	BM [-]	$\dot{m}$ [-]	ψ [-]
0.2	393	0.3	6,000	1.454	1.18	18.94	0.31	0.025	15

The results of the steady-state simulation of the flow have been transferred to conduct the structural analysis of the turbine impeller in transient conditions. The thermal loads are varied on each pocket wall of the impeller cyclically in time at the imposed rotational speed. Hence, each pocket of the impeller is subjected to all the thermal loads calculated from the CFD during one round. The pressure and temperature distributions presented in Figure 2 are the results of the CFD simulation that were used as inputs to the structural analysis.

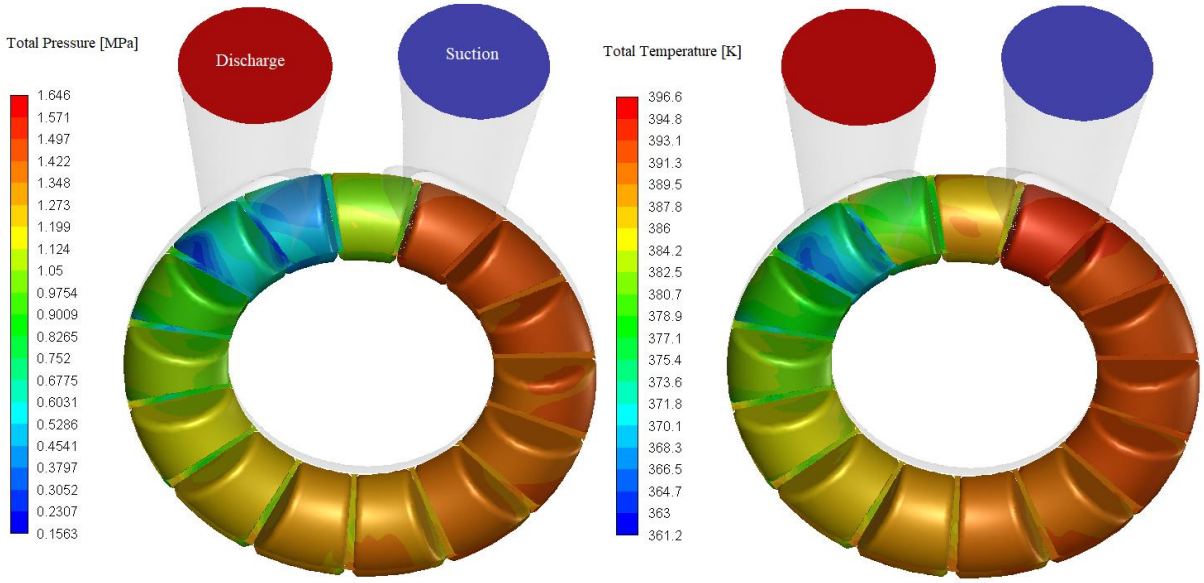

Figure 2: Contours of the total pressure (left) and the total temperature (right).

2.2 Methods of the analysis

The results of the CFD model were transferred to a thermo-structural model applied to the turbine impeller and carried out in ANSYS® Mechanical. For the sake of the scope, the most severe operating condition was considered which occurs when the material of the turbine is at ambient temperature and the inlet conditions of the working fluid are as reported in Table 1. For each impeller pocket, the average values of the convection heat transfer coefficients and the temperatures of the fluid were retrieved from the CFD to evaluate the heat transfer rate during the start-up. In the structural analysis, the rotation of the impeller is modeled by changing periodically the imported pressure and temperature contours according to the turbine shaft speed while the impeller domain is maintained fixed. Figure 3 shows the applied convection heat transfer coefficient to an impeller pocket for 10 cycles equivalent of 0.1 s.

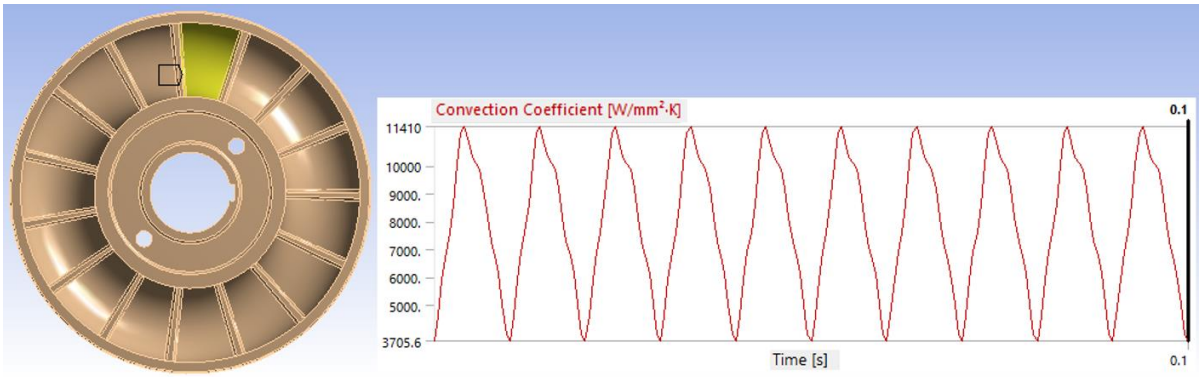

Figure 3: The convection heat transfer coefficient applied cyclically to each impeller pocket (e.g. the one highlighted in yellow).

With the final aim of realizing a cheap expander, two different materials were considered: wrought aluminum and polyphenylene sulfide (PPS) with 30% of glass content. The former is typically used in the manufacturing of jet engine impellers and compressor rings (ASM International Handbook Committee, 1990), while the latter is a techno-polymer with excellent thermal properties, like high temperature and chemical resistance, precision moldability and dimensional stability (Park and Chun, 1996). The thermal and mechanical properties of the two investigated materials are reported in Table 2.

Table 2: Properties of the selected materials for thermo-structural analysis

Properties	**Aluminum 2124-T851**	**PPS GF30**
Density [kg/m^3]	2770	1960
Thermal conductivity [W.m^{-1}.K^{-1}]	165	0.258
Specific Heat [J.kg^{-1}.K^{-1}]	875	1440
Coefficient of thermal expansion [K^{-1}]	24e-6	35e-6
Young's Modulus [MPa]	70000	5000
Yield Stress at 373 K [MPa]	412	100

Therefore, the thermal transient behavior of the impeller has been studied for both materials. Then, the temperature distribution in the impeller body obtained from the transient thermal simulation is used as the input to the structural model in combination with the pressure distribution from the CFD model.

3 RESULTS AND DISCUSSION

3.1 The Thermal Transient Analysis

The transient thermal analysis shows that the aluminum impeller reaches the thermal equilibrium in about 10 s, while the PPS one shows a nearly constant average temperature after 15 minutes as presented in Figure 4.

In addition, the aluminum impeller reaches a fairly uniform temperature distribution, while the PPS impeller shows a rather homogeneous temperature distribution only in the pockets that are in contact with the fluid, and the center of the impeller that is in contact with the shaft has a much lower temperature as shown in Figure 5. This marked difference is caused by the very low thermal conductivity of the PPS material compared to the aluminum, which results in a low heat transfer from the fluid to the center of the impeller.

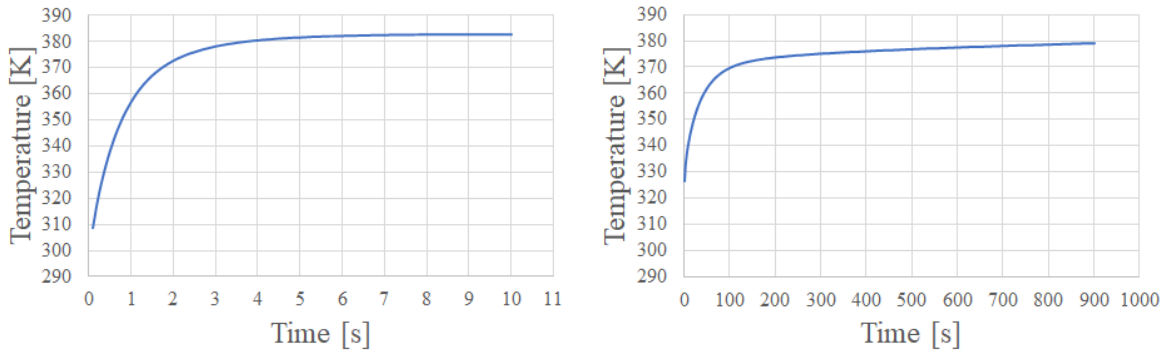

Figure 4: The average temperature of the entire impeller with time for aluminum (left) and PPS (right).

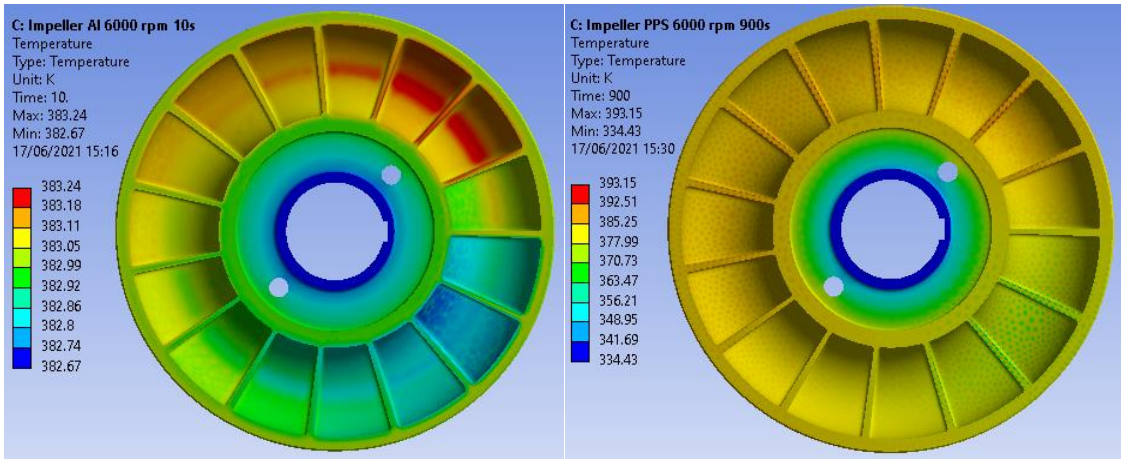

Figure 5: The temperature distribution at the steady state for aluminum (left) and PPS (right).

3.2 **The Structural Analysis**

The transient thermal results previously obtained have been transferred into the structural model together with the pressure distribution obtained from the CFD analysis. In addition, the impeller rotational speed (6000 rpm) is set as the centrifugal load, while a displacement constraint, in cylindrical coordinates, is considered at the surface in contact with the shaft. The details of the thermo-mechanical model are shown in Figure 6.

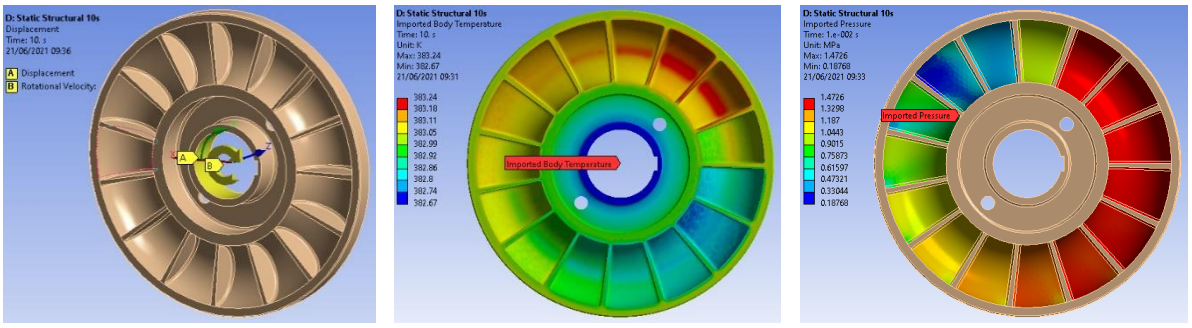

(a) (b) (c)

Figure 6: Thermo-mechanical model: (a) boundary conditions; (b) transient thermal results and (c) pressure distribution (imported from CFD)

The structural analysis aims at assessing the maximum stress, the reaction moment, and the expansion of the material that may result in the critical operation of the impeller.

Under the thermal steady-state conditions, the simulation gives maximum stress (Von Mises equivalent) on the aluminum impeller equal to 42 MPa, while the result is similar for the PPS impeller, with a

maximum stress of about 40 MPa as represented in Figure 7. The similarity between these peak values, as well as of the stress distribution in general, is indicative of the fact that the impeller has achieved a steady-state operating condition. Indeed, at the steady-state condition, the main difference in the load is ascribable to the inertial load of the impeller due to the different densities of the materials.

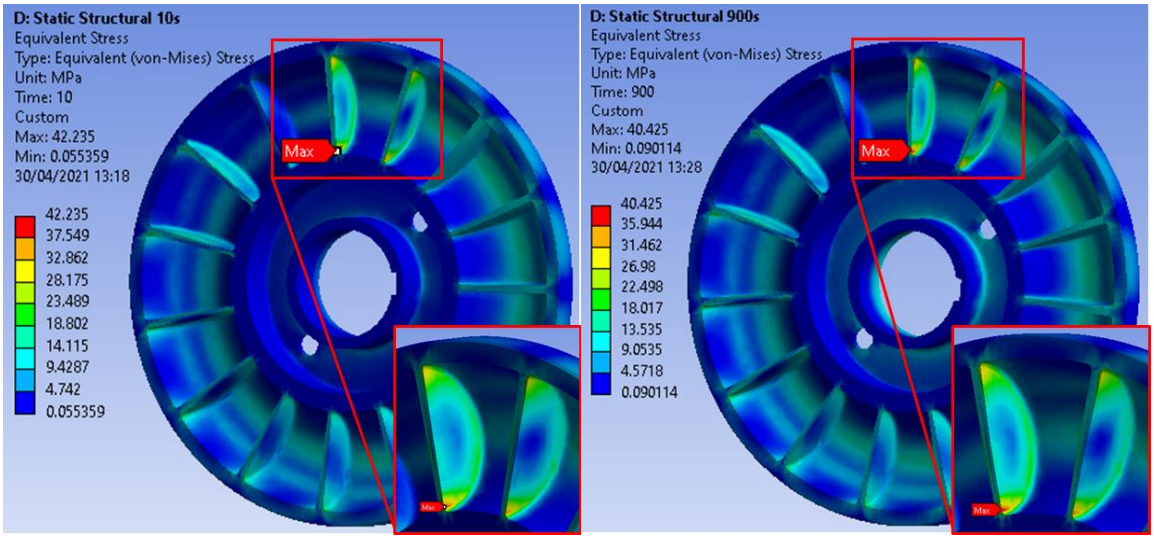

Figure 7: Von-Mises stress distribution at the steady-state for aluminum (left) and PPS (right).

However, the maximum stress on the impeller is achieved during the transient thermal phase as reported in Figure 8. During the start-up, the impeller is subjected to a peak of stress which occurs at 0.9 s for aluminum and 13.5 s for PPS. This peak is observed at the surface in contact with the shaft and it corresponds to a value of 127.4 MPa and 50.8 MPa for aluminum and PPS respectively. Even though these values are higher than the maximum stress achieved during the steady-state condition, they are far from the Yield Stress of each material reported in Table 2. Moreover, the fluctuation of the stress for the aluminum impeller is considerably higher than that of the PPS due to the significantly higher thermal conductivity of aluminum resulting in a more severe temperature difference inside the impeller during the transient heat up of the impeller. In Figure 8a the abrupt change of the stress slope is associated to the change in the position of the maximum stress node in the model.

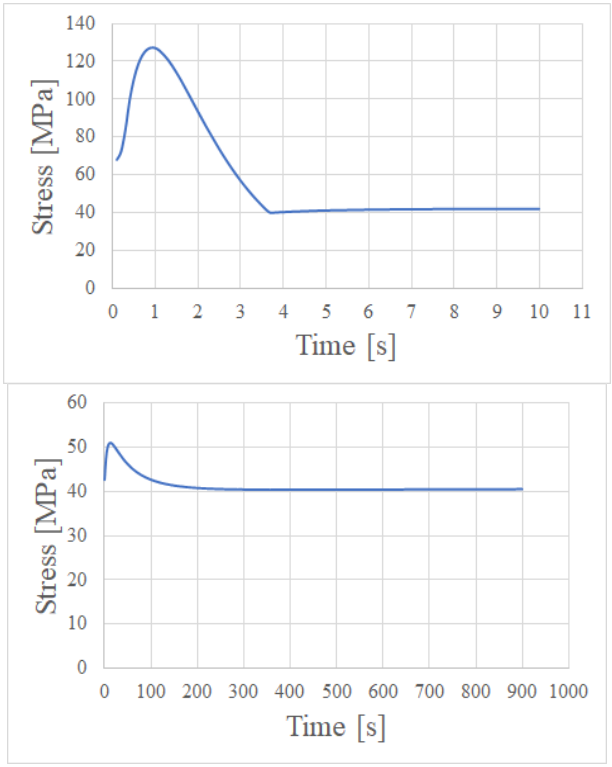

Figure 8: The maximum equivalent stress (nodal probe) in the impeller with time for aluminum (left) and PPS (right).

Then, the reaction moment at the shaft contact surface is calculated. In particular, a maximum axial moment of 1.586 Nm is obtained. Therefore, considering the shaft speed of 6000 rpm, the corresponding shaft power output about 1 kW for half of the turbine considered in this study.
Eventually, the analysis has pointed out that the maximum radial displacement occurs at the outer diameter, and it corresponds to about 0.07 mm and 0.14 mm for aluminum and PPS respectively. This difference is mainly due to the differing Young's modulus and the thermal expansion coefficients of the two materials.

4 CONCLUSIONS

In this work, a structural analysis of an RFT to be used in ORC systems for low-grade waste heat recovery (WHR) applications has been performed in ANSYS Mechanical considering a working fluid inlet temperature of 393 K, a mass flow rate of 0.2 kg/s, and a shaft speed of 6000 rpm. Two different materials of the impeller have been considered namely wrought aluminum and PPS to realize a low-manufacturing cost expander.
A transient thermal model has been adopted considering the results of a previous CFD study to calculate the temperature distribution and estimate the required time to reach the steady-state condition for both materials. Then, a structural model has been adopted using the transient temperature distribution from the transient thermal model and pressure distribution from the steady-state CFD model.
The performed structural analysis has shown that the maximum tensile strength is about 127.4 MPa and 50.8 MPa for aluminum and PPS respectively during the turbine start-up from the ambient temperature that is due to the different thermal conductivities of the considered materials. Under thermal steady-state conditions, instead, the maximum stress lowers to 42 MPa for aluminum and 40 MPa for PPS. The difference is because of different densities of the materials resulting in different centrifugal forces. Furthermore, an expected power output of 2 kW has been obtained considering both sides of the impeller rotating at 6000 rpm neglecting all the mechanical losses. Furthermore, a radial displacement of about 0.07 mm and 0.14 mm at the outer diameter has been estimated for aluminum and PPS respectively. Therefore, the present investigation has provided useful insights to support the further fluid dynamics optimization of the expander before its manufacturing.

NOMENCLATURE

$\dot{M}$	mass flow rate	(kg/s)
$\dot{m}$	reduced mass flow rate	(-)
n	impeller speed	(rpm)
w	impeller frequency	(rad/s)
P	pressure	(MPa)
T	temperature	(K)
$\dot{W}$	power (work)	(kW)
η	efficiency	(%)
ψ	stage loading	(-)
BM	Blade Mach number	(-)
U	impeller velocity	(m/s)
D	impeller tip diameter	(m)
C	speed of sound	(m/s)
C_p	specific heat	($J/kg^{-1}.K^{-1}$)

abbreviations

PPS	polyphenylene sulfide
RFT	Regenerative Flow Turbine
WHR	Waste Heat Recovery
CFD	Computational Fluid Dynamics
rpm	round per minute

Subscripts

in	inlet
is	isentropic
out	outlet
t	turbine
th	thermodynamic
tts	total-to-static
0	total

ACKNOWLEDGEMENT

The authors wish to thank S.TRA.TE.G.I.E. Srl (www.strategiesrl.com) for its support in the drawing of the RFT under investigation.

REFERENCES

2021 ANSYS® Academic Research CFD, Release 21:

ASM International Handbook Committee, 1990. *ASM Handbook Volume 2: Properties and Selection: Nonferrous Alloys and Special-Purpose Materials - ASM International*: ASM International.

Dixon, S.L., Hall, C.A., 2010. *Fluid Mechanics and Thermodynamics of Turbomachinery*: Elsevier Inc, University of Cambridge, Cambridge, UK.

Dumont, O., Parthoens, A., Dickes, R., Lemort, V., 2018. Experimental investigation and optimal performance assessment of four volumetric expanders (scroll, screw, piston and roots) tested in a small-scale organic Rankine cycle system: *Energy*,.

Johnson, I., Choate, W.T., Davidson, A., 2008. Waste Heat Recovery: Technology and Opportunities in U.S. Industry.:

Mahmoudi, A., Fazli, M., Morad, M.R., 2018. A recent review of waste heat recovery by Organic Rankine Cycle: *Appl. Therm. Eng.*,.

Moradi, R., Cioccolanti, L., Bocci, E., Villarini, M., Renzi, M., 2019. Numerical Investigation on the Performance of a Regenerative Flow Turbine for Small-Scale Organic Rankine Cycle Systems: *J. Eng. Gas Turbines Power*, vol. 141, no. 9: .

Moradi, R., Habib, E., Bocci, E., Cioccolanti, L., 2020. Investigation on the use of a novel regenerative flow turbine in a micro-scale Organic Rankine Cycle unit: *Energy*, vol. 210, p. 118519.

Park, H.J., Chun, B.C., 1996. Effect of temperatures on the mechanical and morphological properties of polyphenylene sulfide composites: *Polym. Bull.*, vol. 37, no. 1: p. 103–110.

Quail, F.J., Scanlon, T., Strickland, M., 2010. Development of a regenerative pump impeller using rapid manufacturing techniques: *Rapid Prototyp. J.*, vol. 16, p. 337–344.